

Inelastic neutron scattering study of the localized dynamics of protons in KHCO_3 single crystals

Susumu Ikeda

High Energy Accelerator Research Organization, Tsukuba, Ibaraki, Japan

Shoji Kashida

Department of Physics, Faculty of Science, Niigata University, Niigata, Japan

Hidehiko Sugimoto

Department of Physics, Faculty of Science and Engineering, Chuo University, Kasuga, Bunkyo-ku, Tokyo, Japan

Yasusada Yamada

Advanced Research Center for Science and Engineering, Waseda University, Okubo, Shinjuk-ku, Tokyo, Japan

S. M. Bennington

ISIS, Daresbury and Rutherford Appleton Laboratory, Chilton, Didcot, Oxon, OX11 0QX, United Kingdom

François Filliaux*

LADIR-CNRS, UMR 7075 Université P. et M. Curie, 2 Rue Henry Dunant, 94320 Thiais, France

(Received 28 January 2002; revised manuscript received 8 July 2002; published 15 November 2002)

In the crystal of potassium hydrogen carbonate (KHCO_3) all $\text{OH}\cdots\text{O}$ hydrogen bonds are equivalent and virtually parallel to each other. The inelastic incoherent scattering function measured with oriented single crystals is presented as maps of intensity for energy transfer values corresponding to proton vibrations. All maps resemble those anticipated for harmonic oscillators with effective masses close to 1 amu. Contributions from the lattice dynamics, vibrational coupling with heavy atoms, anharmonicity, mixing of states, and Fermi resonance are analyzed. It is concluded that anharmonicity plays a major role and proton dynamics cannot be represented with normal coordinates within the harmonic force-field approximation.

DOI: 10.1103/PhysRevB.66.184302

PACS number(s): 63.20.Pw, 25.40.Fq, 33.20.Tp, 78.70.Nx

I. INTRODUCTION

In attempting to account for vibrational spectra, it is widely accepted that dynamics of atoms and molecules are reasonably well represented with quantized normal coordinates arising from harmonic force-fields which describe to a certain approximation complex multidimensional potentials in molecules and crystals.¹⁻⁶ The determination of such force-fields requires a full analysis of spectral profiles: the normal frequencies give the eigenvalues of the dynamical matrix, and the band intensities are related to the eigenvectors. However, owing to the complexity of interaction of photons with matter, band intensities measured with optical techniques (namely, infrared and Raman) cannot be fully exploited because the relevant transition moment operators are largely unknown and they are poorly calculated even with the most advanced quantum chemistry methods. Consequently, force fields refined with respect to the observed frequencies only are largely underdetermined, even when complementary information is obtained from other types of experiments.

This difficulty is partially overcome with the incoherent inelastic neutron scattering (INS) technique. The intensity for a normal mode is related to the mean square amplitude of displacement (MSD) scaled by the nuclear cross section for each atom. The incoherent scattering cross section for protons being about one order of magnitude greater than for any other atom, the measured intensity for hydrogenous samples

is virtually proportional to the scattering function for hydrogen atoms. In principle, the dynamics of other atoms remain largely unknown. However, within the force-field representation, the mean position of a hydrogen atom oscillating at a high frequency (internal mode) follows adiabatically the slow lattice vibrations corresponding to translational and librational motions of the heavy molecular entities. This proton riding enhances the intensity for the lattice modes and thus provides information on these dynamics.

For rather “soft” molecular crystals, the lattice and internal vibrations are well separated and the total scattering function that is measured can be written as a convolution of the scattering functions for the lattice and internal modes, respectively,⁷⁻¹³

$$S(\mathbf{Q}, \omega) = S_L(\mathbf{Q}, \omega) \otimes S_M(\mathbf{Q}, \omega). \quad (1)$$

The momentum transfer vector is $\mathbf{Q} = \mathbf{k}_0 - \mathbf{k}_f$ with $|\mathbf{k}_0| = 2\pi/\lambda_0$ and $|\mathbf{k}_f| = 2\pi/\lambda_f$, where λ_0 and λ_f are the incident and scattered wavelengths, respectively. The neutron energy transfer is $\hbar\omega$. The band intensity for each internal vibrational mode is depressed by the lattice Debye-Waller factor $\exp[-2W_L(\mathbf{Q})]$ and the missing intensity is redistributed amongst phonon wings corresponding to combinations with the lattice modes.¹⁴ Consequently, the zero-phonon transition of intramolecular modes at high energy and momentum transfer should be hardly visible and the spectral profile should be dominated by phonon-wings. However, in some

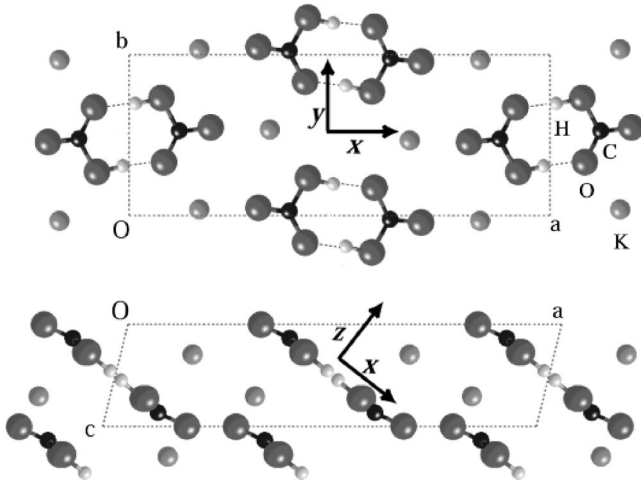


FIG. 1. Schematic view of the crystalline structure of KHCO_3 at 14 K after Ref. 17. The carbonate moieties linked by moderately strong hydrogen bonds with length $\text{O}\cdots\text{O}=2.59$ Å from planar centrosymmetric dimer entities $(\text{HCO}_3^-)_2$ (Refs. 15–17). The dimers are located at C_i sites with their midplanes parallel to the $(\bar{3}01)$ planes, at 42° with respect to the (a,b) planes. The structure remains unchanged from 298 K to 14 K and there is no proton disorder at low temperature.

molecular crystals internal modes at high frequency are clearly observed for surprisingly large Q -values. For example CH stretching modes for a crystal of hexamethylenetetramine were observed at ≈ 2900 cm^{-1} for $|\mathbf{Q}| > 13$ Å $^{-1}$.^{8–11} In that case, the decoupling of internal and external motions was supposed to be a consequence of the very large frequency ratio for these modes.

The potassium hydrogen carbonate (KHCO_3) crystal (Fig. 1) has also revealed significant decoupling of the internal and lattice modes. In this prototypical system for INS studies all protons are equivalent and hydrogen bonds are virtually parallel to each other.^{15–17} Vibrational spectra of KHCO_3 and KDCO_3 have been thoroughly investigated.^{18–23} The INS spectrum of KHCO_3 is rather simple. It is largely dominated by the internal bending modes of the protons. However, the spectral profile could not be represented with conventional harmonic force-fields based on the valence bond picture.²¹ The intensity observed for lattice-modes below 200 cm^{-1} is rather weak compared to the proton bending modes (for example, at ≈ 1000 and 1350 cm^{-1}) and this was regarded as straightforward evidence that dynamics for protons and heavy atoms are largely decoupled. This conclusion was further confirmed by simulation of the spectral profile with empirical force-fields. The spectra were best represented with localized proton modes in a “fixed” (laboratory) referential frame. The bending modes of the protons are independent of both hydrogen bond and CO_3^{2-} vibrations and the effective oscillator masses are equal to 1 amu. So far, the physical origin of these dynamics is not well established. On the other hand, the INS spectral profile in the 200 cm^{-1} region is more ambiguous since intensity arising from mixing of the OH and $\text{O}\cdots\text{O}$ stretching coordinates cannot be distinguished from the tunnelling transition, anticipated in the same frequency range, for proton transfer within a qua-

sisymmetric double-well potential.

Because the crystal structure and vibrational spectra evidence rather weak interaction between dimeric entities, KHCO_3 can be regarded as a test example for modelling with quantum chemistry methods. However, we are not aware of any published simulation of the vibrational dynamics for this system. To the best of our knowledge, even the most advanced methods for quantum mechanical calculations of force-fields for such hydrogen bonded systems have not yet reached the level of accuracy required for direct comparison with the observed spectra.

In order to obtain a more focused view of the proton dynamics we have carried out new INS measurements, over rather large momentum and energy transfer ranges, on single crystals of KHCO_3 . These experiments are complementary to previous measurements^{21,22} of a narrow slice of the (\mathbf{Q},ω) space along the trajectory $\hbar\omega \approx \hbar^2|\mathbf{Q}|^2/2m_n$, where m_n is the neutron mass.²⁴ With these new data we can determine the MSD's of H atoms and the effective oscillator mass for each internal mode. Furthermore, we can analyze the consequences of usual concepts of vibrational spectroscopy (normal coordinates, mixing of states, Fermi resonance) to the scattering function.

In the next section the approximations used for the analysis of the scattering function are presented. Experimental details are given in Sec. III. In Sec. IV partial views of the measured scattering function are presented as maps of intensity for the internal transitions involving significant displacements of H atoms. Fundamentals, overtones and combinations are distinguished. In the last section (V) the MSD's estimated for each mode are compared to those for harmonic oscillators. The contribution of anharmonic coupling and Fermi resonance is also presented. Finally, we conclude that anharmonic coupling between excited vibrational states offers a better representation of the internal dynamics of KHCO_3 dimers than the usual normal coordinates.

II. THE PROTON CRYSTAL APPROXIMATION

From the standpoint of the INS spectrum, KHCO_3 can be regarded to a good approximation as a crystal of equivalent protons so weakly coupled to the surrounding atoms that the framework of carbonate and potassium ions can be virtually ignored.²¹ The dynamical model is thus greatly simplified. At low temperature ($kT \ll \hbar\omega_{if}$), the scattering function for uncoupled protons including multiple phonon-creation processes can be rewritten as

$$S_H(\mathbf{Q},\omega) = |\langle \Psi_f(\mathbf{r}) | \exp(i\mathbf{Q}\cdot\mathbf{r}) | \Psi_i(\mathbf{r}) \rangle|^2 \delta(\omega - \omega_{if}), \quad (2)$$

where Ψ_i and Ψ_f are the wave functions, depending on the spatial coordinate \mathbf{r} , in the initial and final states, respectively. INS spectral profiles in \mathbf{Q} measured at energy transfer $\hbar\omega_{if}$ contain spatial information on the wave functions Ψ_i and Ψ_f , and thus on the effective potential $V(\mathbf{r})$ experienced by H atoms.²⁵ This information cannot be obtained with optical techniques limited to negligibly small $|\mathbf{Q}|$ values. This information could not be obtained either in previous INS

experiments.²¹ Moreover, with powdered samples it was impossible to determine the spatial orientation of the displacement vectors for H atoms.

In the KHCO_3 crystal the proton modes are parallel to the principal axes of the dimers: x for the stretching (ν OH), y for the in-plane bending (δ OH), and z for the out-of-plane bending (γ OH), as shown in Fig. 1.^{22,23} Within the harmonic approximation, the proton wave functions $\Psi_n(\mathbf{r})$ can be factorized as $\Psi_{n_x}(x)\Psi_{n_y}(y)\Psi_{n_z}(z)$ and the scattering function for the $|0\rangle \rightarrow |n_\alpha\rangle$ transition of an isolated harmonic oscillator in 1D is

$$S_{n_\alpha}(Q_\alpha, \omega) = \frac{(Q_\alpha^2 u_{0\alpha}^2)^{n_\alpha}}{n_\alpha!} \exp(-Q_\alpha^2 u_{0\alpha}^2) \delta(\omega - n_\alpha \omega_{0\alpha}),$$

$$\alpha = x, y \text{ or } z. \quad (3)$$

The mean-square amplitude $u_{0\alpha}^2$ in the ground state depends on the mass m and frequency $\hbar \omega_{0\alpha}$ as

$$u_{0\alpha}^2 = \langle \Psi_0(\alpha) | \alpha^2 | \Psi_0(\alpha) \rangle = \frac{\hbar}{2m\omega_{0\alpha}}. \quad (4)$$

The scattering function for the $|000\rangle \rightarrow |n_x n_y n_z\rangle$ transition in a single crystal of protons can be written as

$$S_H(Q_x, Q_y, Q_z, \omega) = \bar{S}_{n_x}(Q_x) \times \bar{S}_{n_y}(Q_y) \times \bar{S}_{n_z}(Q_z) \\ \times \delta[\omega - (n_x \omega_{0x} + n_y \omega_{0y} + n_z \omega_{0z})]; \quad (5)$$

with the scattering amplitude,

$$\bar{S}_{n_\alpha}(Q_\alpha) = \frac{(Q_\alpha^2 u_{0\alpha}^2)^{n_\alpha}}{n_\alpha!} \exp(-Q_\alpha^2 u_{0\alpha}^2), \quad \alpha = x, y \text{ or } z. \quad (6)$$

For $Q_\alpha^2 u_{0\alpha}^2 = n_\alpha$, the intensity is a maximum proportional to $(n_\alpha^{n_\alpha}/n_\alpha!) \exp(-n_\alpha)$.

The powder averaged density of states for lattice modes in KHCO_3 can be represented with a broad continuum centered at $\approx 100 \text{ cm}^{-1}$ and a full width at half height of $\approx 100 \text{ cm}^{-1}$.²¹ For a powdered sample phonon wings should appear as a regular progression of side bands shifted upwards by 100, 200, 300, . . . cm^{-1} with respect to the zero-phonon component. For measurements performed with a single crystal a full analysis of the lattice anisotropic density-of-states should be necessary to account for phonon-wings.

We have measured the scattering function of KHCO_3 for various planes in reciprocal space: (Q_i, Q_j) and $Q_k = 0$, with i, j or $k = x, y$ or z . For each transition the intensity was integrated over a rather narrow slice in energy transfer of $\pm 40 \text{ cm}^{-1}$, which is largely free of phono-wing contributions. Any influence from the lattice modes will be to increase the impact of the Debye-Waller factor in suppressing intensity and this will become more apparent at the higher values of Q .

Graphics views of the maps of intensity for energy transfer values corresponding to proton modes confirm the orientation of the displacement vectors. Fitting procedures yield

the effective MSD (u_α^2) for each vibration and the effective oscillator mass obtained with Eq. (4). It transpires that proton dynamics for the bending modes correspond very closely to isolated harmonic oscillators with a mass of 1 amu. In addition, the Q -profiles provide direct information on the vibrational wave function and phenomena arising from anharmonic coupling terms are tentatively analyzed.

III. EXPERIMENTAL DATA

Three single crystals with cylindrical shapes (diameter $\approx 1 \text{ cm}$, length $\approx 3 \text{ cm}$) have been studied at 20 K. The cylinder axes were oriented either perpendicular to the dimer planes (sample I) or parallel to the b or a crystal axes (samples II and III, respectively). Elastic scattering measurements performed on the same samples were reported previously.²³ It was shown that multiple elastic scattering effects are negligible, owing to the sample geometry and to the characteristics of the spectrometer. Multiple scattering events involving inelastic processes are even less probable.

The MARI spectrometer at the ISIS pulsed neutron source²⁶ is a direct geometry spectrometer. The detectors continuously cover angles from 3° to 135° , all with the same length of secondary flight path. The incident energy was $E_i \approx 4000 \text{ cm}^{-1}$ ($\lambda_i \approx 0.4 \text{ \AA}$) with a resolution $\Delta E_i/E_i \approx 2\%$. For each sample, dimer planes were either parallel or perpendicular to the plane containing the detector bank and the incident beam.

Measurements were carried out in such a way that \mathbf{Q} was either parallel ($Q_z = 0$) or perpendicular (Q_x or $Q_y = 0$) to the mean plane of the dimers (Fig. 1). For each sample, the orientation of the crystal with respect to the incident beam was changed from 0 to 180° , by steps of 15° , in order to probe a half-plane in reciprocal space. The time-of-flight data were converted from counts per channel per angle to $S(Q_i, Q_j, \omega)$ with standard procedures.²⁷ For each run the detectors were grouped together into roughly equal Q -bins. A cylindrical vanadium sample was measured in order to correct for detector efficiency and solid angle. A few poor detectors were eliminated. The background obtained without sample in the beam was subtracted. The $S(\phi, \omega)$ was created with the SPEAL code and then converted into the $S(Q_i, Q_j, \omega)$.²⁶ In order to improve the signal to noise ratio, the data were rebinned with $\Delta \hbar \omega = 40 \text{ cm}^{-1}$ and $\Delta Q = 1 \text{ \AA}^{-1}$.

The symmetrized maps of intensity obtained at various energy-transfer values $\hbar \omega$ are referred to as $S(Q_x, Q_y, \omega)$, $S(Q_x, Q_z, \omega)$ and $S(Q_y, Q_z, \omega)$, for samples II, III, and I respectively. According to the crystal structure the OH bonds are not exactly aligned to the Q_x direction (Fig. 1), but the small deviations give only a marginal uncertainty on the eigenvector orientation for each mode.

As long as the energy of incident neutrons remains small compared to the dissociation energy of the protons, the scattering function for any transition depends only on energy and momentum transfer values. The incident energy of 4000 cm^{-1} used in the experiments with the MARI spectrometer is fully compatible with this approximation. Therefore, the data presented below refer to the same scattering function as

that measured previously over a much more limited momentum transfer range.²¹

IV. MAPS OF INTENSITY

In the KHCO_3 crystal the contribution of intra and interdimer coupling terms can be distinguished with optical and INS techniques. Symmetry species arising from intradimer terms are infrared (B_u) or Raman (A_g) active. The splitting ranges from 60 to 40 cm^{-1} for proton vibrations.^{18–20} With INS, there is no symmetry-related selection rules and both species contribute to the spectra. However, in the experiments under consideration in this present report, the band splitting were not resolved and intradimer coupling terms were ignored.

The INS technique probes the density-of-states arising from interdimer coupling terms, whilst optical techniques are specific to the center of the Brillouin zone. As the INS bands and their counterparts in the infrared have similar breadths, interdimer coupling terms are negligible. Therefore, proton dynamics are represented with single proton oscillators in the remainder of this work.

A. OH bending

The maps of intensity for the bending modes (see Figs 2–6) are in good agreement with Eq. (5). Within experimental errors, the proton displacement vectors for the normal modes are parallel to the x , y and z directions.

For the γ OH at 960 cm^{-1} ,^{18–21} the maps correspond to those anticipated for the $|000\rangle \rightarrow |001\rangle$ transition (see Figs. 2 and 3). Elastic scattering is observed along Q_y (Fig. 2) or Q_x (Fig. 3). There is no visible inelastic contribution along Q_x or Q_y .

The bands at 1360 and 1600 cm^{-1} have been assigned to coupled displacements along the δ OH and carbonate stretching coordinates ($\nu_a \text{ CO}_3$ and $\nu'_a \text{ CO}_3$, respectively).^{18–21} However, the maps presented in Figs. 4, 5, and 6 are very close to the ideal scattering function for the $|000\rangle \rightarrow |010\rangle$ transition of a proton harmonic oscillator. The intensity observed along Q_x or Q_z at $Q_y=0$ is close to zero within statistical errors. Therefore, contribution of the stretching and out-of-plane bending coordinates to these transitions is doubtful. The effective oscillator masses of ≈ 1 amu are apparently in conflict with previous assignment schemes for these modes. Within the framework of the harmonic force field, the normal coordinates for the modes at 1360 and 1600 cm^{-1} (say s' and s , respectively) should be linear combinations of internal coordinates,

$$s' = u'(\nu'_a \text{ CO}_3) + v'(\delta \text{ OH}) + \dots$$

$$\text{and } s = u(\nu_a \text{ CO}_3) + v(\delta \text{ OH}) + \dots$$

Then, the effective masses for these normal oscillators should be much greater than 1 amu. However, the maxima of intensity at $Q_y \approx 9 \text{ \AA}^{-1}$ in Figs. 4 and 5, and at $Q_y \approx 10 \text{ \AA}^{-1}$ in Fig. 6, correspond to effective masses very close to 1 amu. Therefore, there is no visible contribution of displacements of the C and O atoms. This new assignment

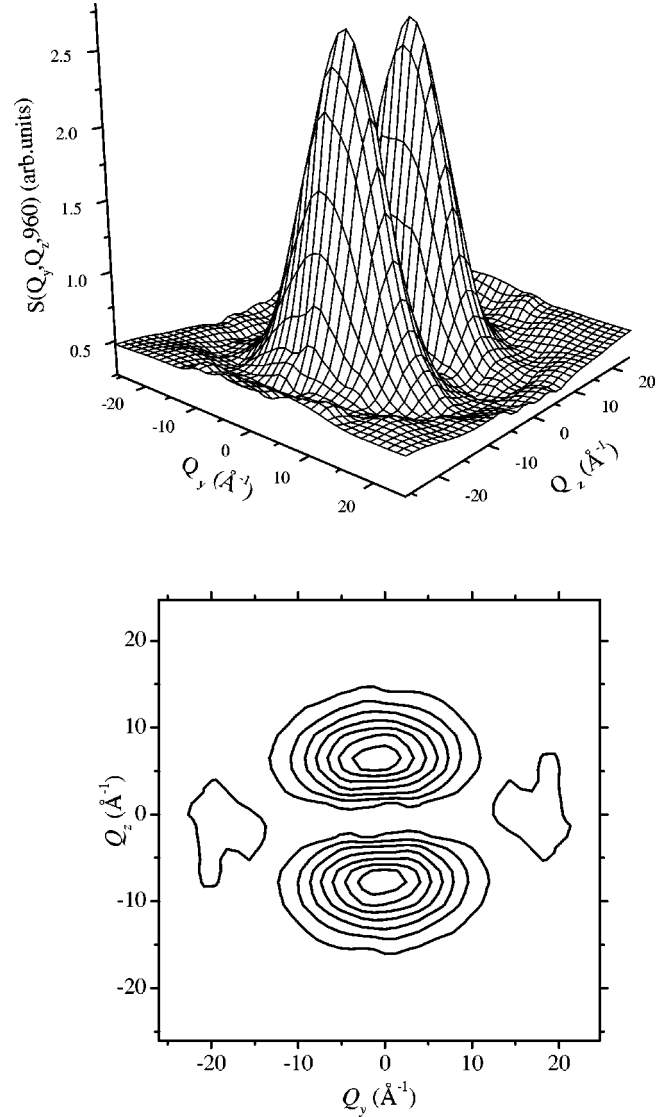


FIG. 2. $S(Q_y, Q_z, 960)$: Q_y is parallel to the dimer planes along the b crystal axis and Q_z perpendicular to the dimer plane. Intensities were integrated over $920 \text{ cm}^{-1} < \hbar\omega < 1000 \text{ cm}^{-1}$. Landscape view (top) and isointensity contour map (bottom).

scheme for the band at 1600 cm^{-1} could not be derived from previous INS experiments. This is a further confirmation of the decoupling of the δ OH and CO_3 coordinates.

As an alternative approach, we suppose that the coordinates $\nu_a \text{ CO}_3$, $\nu'_a \text{ CO}_3$, and $\delta \text{ OH}$ are uncoupled in the ground state and the wave function can be factorized as

$$\Psi_0(\nu_a \text{ CO}_3) \Psi_0(\nu'_a \text{ CO}_3) \Psi_0(\delta \text{ OH}) \dots$$

In the excited states anharmonic coupling terms (see below) may combine the wave functions for the internal coordinates as

$$\Psi_{1600} = [p\Psi_1(\nu_a \text{ CO}_3) + q\Psi_1(\delta \text{ OH}) + \dots] \Psi_0(\nu'_a \text{ CO}_3) \dots$$

and

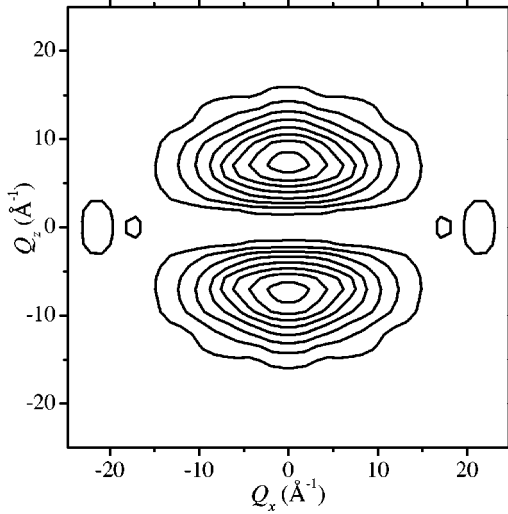
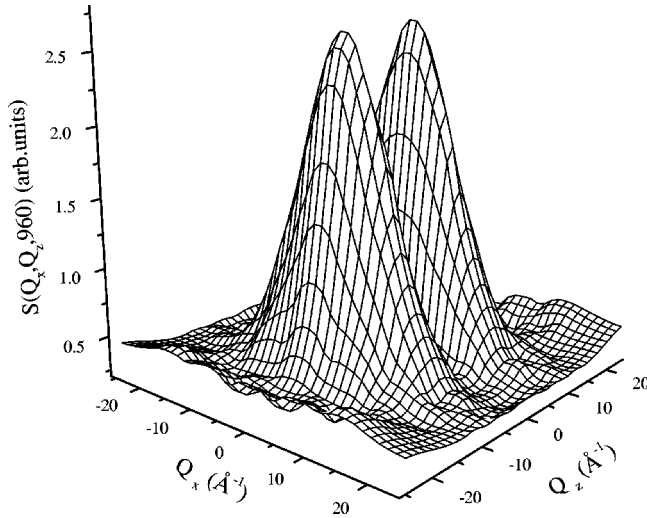


FIG. 3. $S(Q_x, Q_z, 960)$: Q_x is parallel to the dimer and (a, c) planes. Q_z is perpendicular to the dimer plane. Intensities were integrated over $920 \text{ cm}^{-1} < \hbar\omega < 1000 \text{ cm}^{-1}$. Landscape view (top) and isointensity contour map (bottom).

$$\Psi_{1360} = [p' \Psi_1(\nu_a \text{CO}_3) + q' \Psi_1(\delta \text{OH}) + \dots] \Psi_0(\nu_a \text{CO}_3) \dots$$

The contribution of C and O atoms to the total intensity is negligible because of their small cross sections. Moreover, the maximum of the scattering function for such heavy oscillators is at a very large Q value, beyond the measured range. Consequently, the observable part of the scattering function is

$$S(\mathbf{Q}, \omega) \sim q'^2 \bar{S}_1(Q_{\delta \text{OH}}) \delta(\hbar\omega - 1360) + q^2 \bar{S}_1(Q_{\delta \text{OH}}) \delta(\hbar\omega - 1600) + \dots \quad (7)$$

For both transitions, the scattering function is proportional to that of the proton oscillator δOH . As opposed to this, the infrared and Raman bands at 1360 and 1600 cm^{-1} are

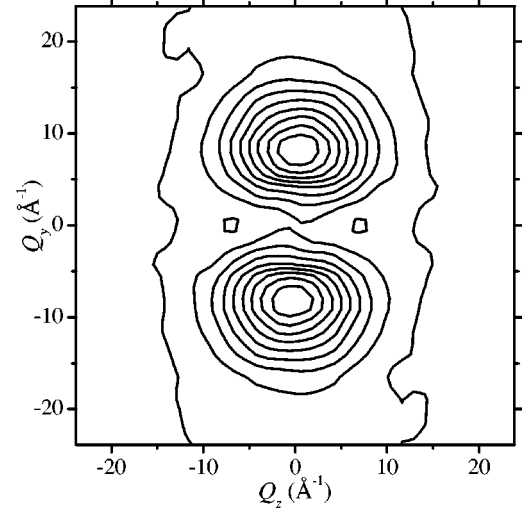
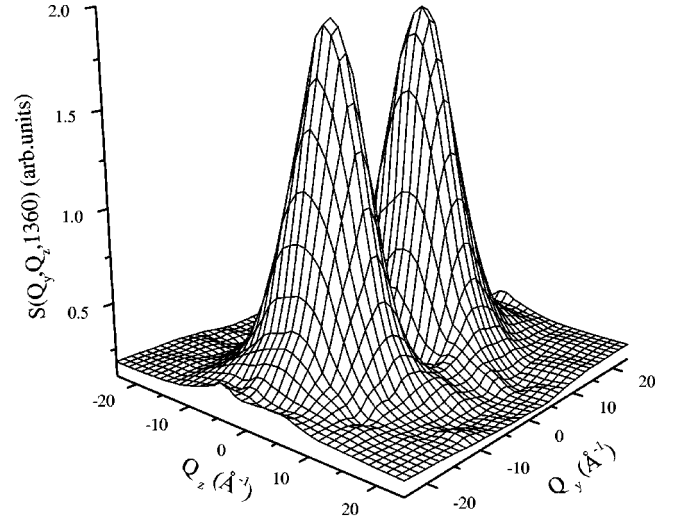


FIG. 4. $S(Q_y, Q_z, 1360)$: Q_y is parallel to the dimer planes along the b crystal axis and Q_z is perpendicular to the dimer plane. Intensities were integrated over $1320 \text{ cm}^{-1} < \hbar\omega < 1400 \text{ cm}^{-1}$. Landscape view (top) and isointensity contour map (bottom).

largely dominated by the CO_3 stretching vibrations which hide the weaker δOH intensity.¹⁸ It appears clearly that bands observed with different techniques at the same frequencies do not correspond necessarily to the same atom displacements.

B. Overtone and combination

For the γOH overtone at $1840 \pm 40 \text{ cm}^{-1}$ the map corresponds to the scattering function for the $|000\rangle \rightarrow |002\rangle$ transition (Fig. 7). Compared to the fundamental transition (Fig. 3) the maxima of intensity along Q_z are shifted from $\approx \pm 7.5$ to $\approx \pm 10.5 \text{ \AA}^{-1}$, as anticipated for an oscillator mass of ≈ 1 amu.

For energy transfer at $(2320 \pm 40) \text{ cm}^{-1}$ the map in the (Q_y, Q_z) plane corresponds to the two-quanta $\gamma \text{OH} + \delta \text{OH}$ combination: $|000\rangle \rightarrow |011\rangle$ (Fig. 8). The four maxima observed at $Q_y \approx \pm 10 \text{ \AA}^{-1}$ and $Q_z \approx \pm 8 \text{ \AA}^{-1}$ with equal intensities could have been anticipated from the product of the

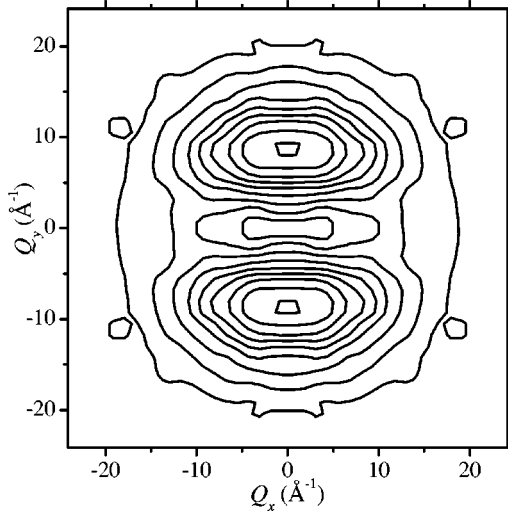
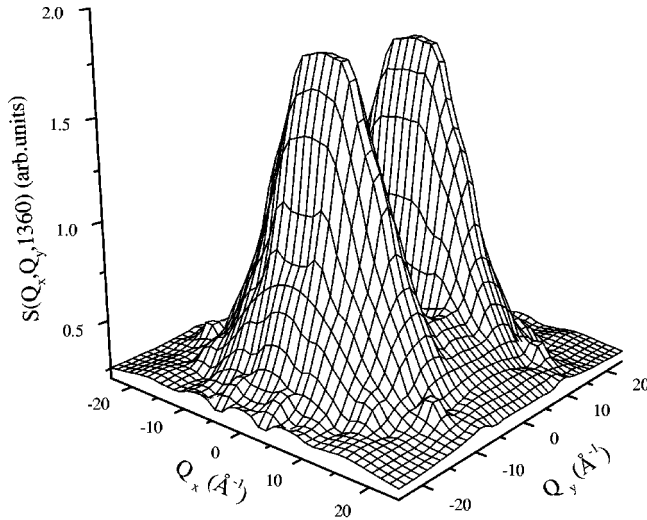


FIG. 5. $S(Q_x, Q_y, 1360)$: Q_x is parallel to the dimer and (a, c) planes. Q_y is parallel to the dimer planes along the b crystal axis. Intensities were integrated over $1320 \text{ cm}^{-1} < \hbar\omega < 1400 \text{ cm}^{-1}$. Landscape view (top) and isointensity contour map (bottom).

scattering functions for the $|000\rangle \rightarrow |001\rangle$ and $|000\rangle \rightarrow |010\rangle$ transitions presented in Figs. 2 and 4.

C. OH stretching

The map for $S(Q_x, Q_y, 2560 \pm 40)$ is a superposition of the scattering functions for the ν OH ($|000\rangle \rightarrow |100\rangle$) and δ OH overtone ($|000\rangle \rightarrow |020\rangle$) (Fig. 9). Relative intensities at maximum along Q_x and Q_y are in proportion to $\sim 1:0.7$, in accordance with the ideal ratio of $1:0.736$ given by Eqs. (5) and (6) for proton oscillators. The mixing of the OH and $\text{O}\cdots\text{O}$ coordinates²¹ is not confirmed.

V. DISCUSSION

A. Mean-square displacements

The MSD's obtained from the best fits, with Eq. (3), to cuts, along Q_x , Q_y or Q_z , of the maps of intensity are gathered in Table I.

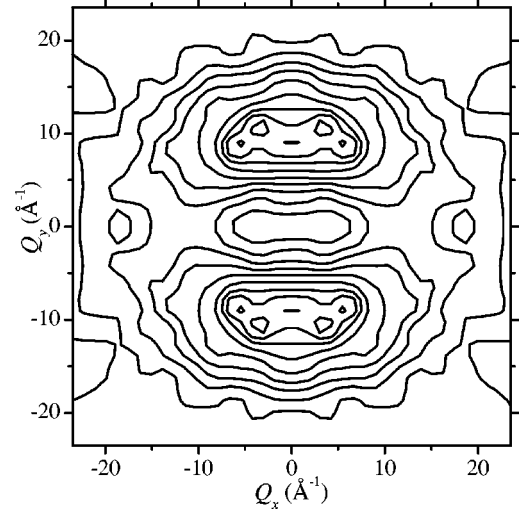
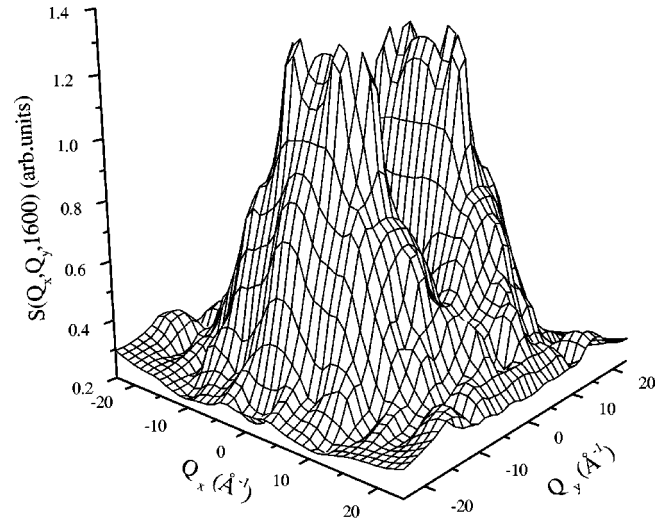


FIG. 6. $S(Q_x, Q_y, 1600)$: Q_x is parallel to the dimer and (a, c) planes. Q_y is parallel to the dimer planes along the b crystal axis. Intensities were integrated over $1560 \text{ cm}^{-1} < \hbar\omega < 1640 \text{ cm}^{-1}$. Landscape view (top) and isointensity contour map (bottom). Owing to the rather poor count statistics intensities were smoothed.

For the γ OH transition the observed profile along Q_z is slightly more depressed at large Q values than anticipated for an isolated-proton harmonic-oscillator [$u_{0z}^2 = 1.75 \times 10^{-2} \text{ \AA}^2$, see Fig. 10(a)], but the difference is not significantly outside the range of statistical errors. The best fit gives $u_z^2 = (1.95 \pm 0.10) 10^{-2} \text{ \AA}^2$ [see Fig. 10(b) and Table I] and an effective mass of (0.9 ± 0.1) amu.

The u_z^2 's obtained for different crystal orientations are quite similar (see Table I). In the (Q_x, Q_z) plane they are virtually identical for the $|000\rangle \rightarrow |001\rangle$ and $|000\rangle \rightarrow |002\rangle$ transitions and, from this standpoint, there is no evidence for potential anharmonicity. In the (Q_y, Q_z) plane the u_z^2 estimated from the $|000\rangle \rightarrow |001\rangle$ transition is slightly greater, whilst the elastic scattering profile of the $|000\rangle \rightarrow |010\rangle$ transition gives a significantly smaller value, very close to that for the harmonic proton oscillator.

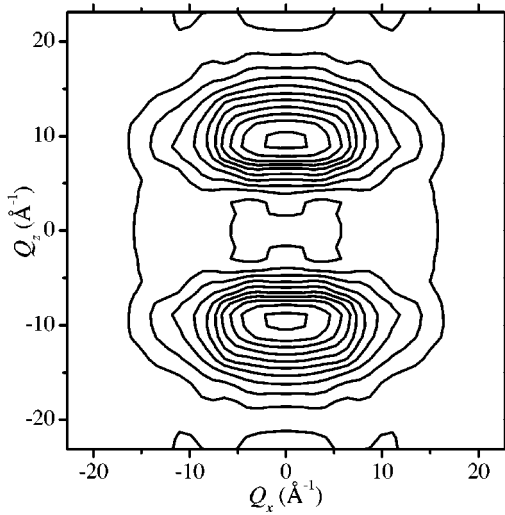
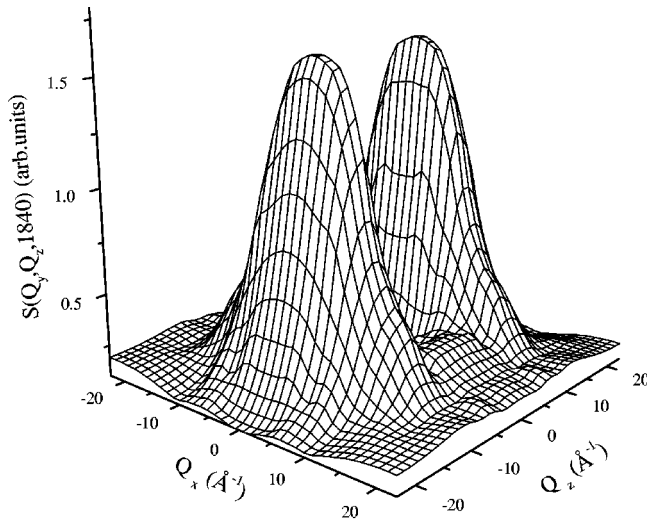


FIG. 7. $S(Q_x, Q_z, 1840)$: Q_x is parallel to the dimer and (a, c) planes. Q_z is perpendicular to the dimer plane. Intensities were integrated over $1800 \text{ cm}^{-1} < \hbar\omega < 1880 \text{ cm}^{-1}$. Landscape view (top) and isointensity contour map (bottom).

The u_z^2 values in Table I cannot be rationalized with the rather weak potential anharmonicity estimated from the comparison of the frequencies for the $|000\rangle \rightarrow |001\rangle$ and $|000\rangle \rightarrow |002\rangle$ transitions. The dispersion of numerical values is likely to reflect experimental imperfections. However, among many sources of error, accidental corruption of the γ OH oscillator by δ OH or ν OH displacements due to misalignment of the samples can be rejected. This should decrease the apparent u_z^2 , compared to u_{0z}^2 . Instead of that, estimated values are systematically greater than u_{0z}^2 . Similarly, multiple scattering events should broaden the observed profiles in Q and give smaller u_z^2 values.

The averaged effective oscillator mass of (0.9 ± 0.05) amu confirms that this mode is very localized and virtually free of mixing with internal coordinates involving heavy atoms. Both the potential anharmonicity and the lattice Debye-Waller factor may decrease the effective mass (increase the

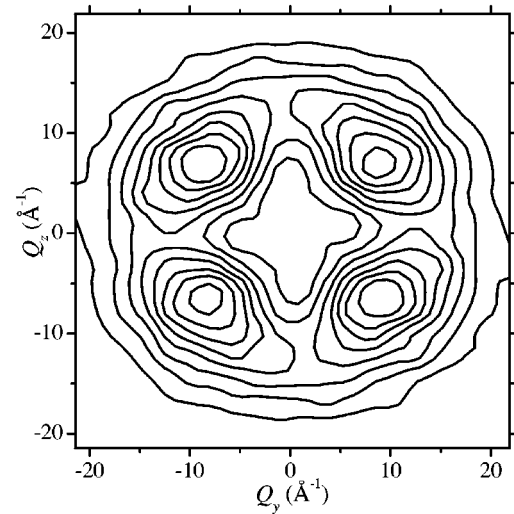
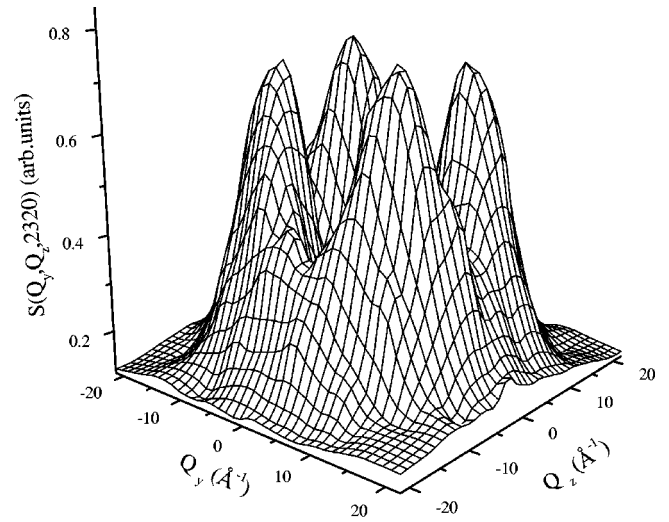


FIG. 8. $S(Q_y, Q_z, 2320)$: Q_y is parallel to the dimer planes along the b crystal axis and Q_z perpendicular to the dimer plane. Intensities were integrated over $2280 \text{ cm}^{-1} < \hbar\omega < 2360 \text{ cm}^{-1}$. Landscape view (top) and isointensity contour map (bottom).

MSD) compared to the bare proton oscillator. However, it is not straightforward to unravel these contributions. To the least, the values $\Delta_z = u_z^2 - u_{0z}^2$ in Table I can be regarded as an upper bound for the contribution of lattice modes to the MSD's for protons.

Similar conclusions apply to the δ OH vibration, albeit with relatively greater statistical errors (see Table I). The MSD's are also systematically greater than anticipated for the harmonic proton oscillator. There is no clear evidence for potential anharmonicity and mixing with internal coordinates involving heavy atoms can be ignored. Therefore, the Δ_y 's could be also representative of the contribution of lattice modes.

For the OH-stretching all Δ_x values but one were obtained from elastic profiles and we have not enough information to account for the very broad band for this mode.^{18-20,28,29}

In order to obtain more confidence in the Δ_α values, a direct estimation of the effective contribution of the lattice

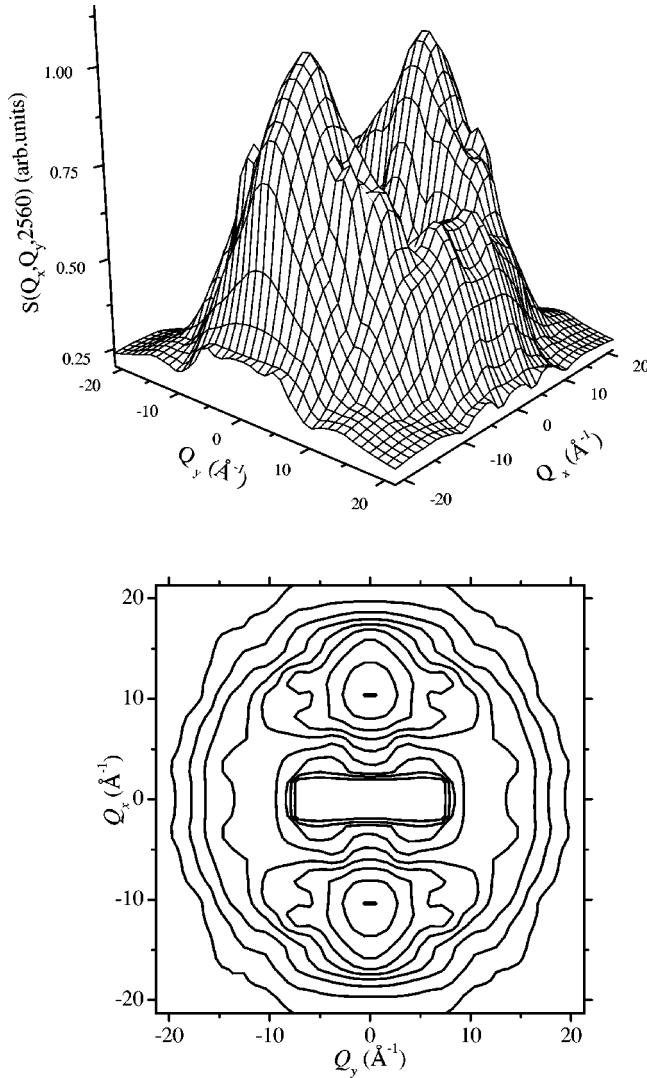


FIG. 9. $S(Q_x, Q_y, 2560)$: Q_x is parallel to the dimer and (a, c) planes. Q_y is parallel to the dimer planes along the b crystal axis. Intensities were integrated over $2520 \text{ cm}^{-1} < \hbar\omega < 2600 \text{ cm}^{-1}$. Landscape view (top) and isointensity contour map (bottom).

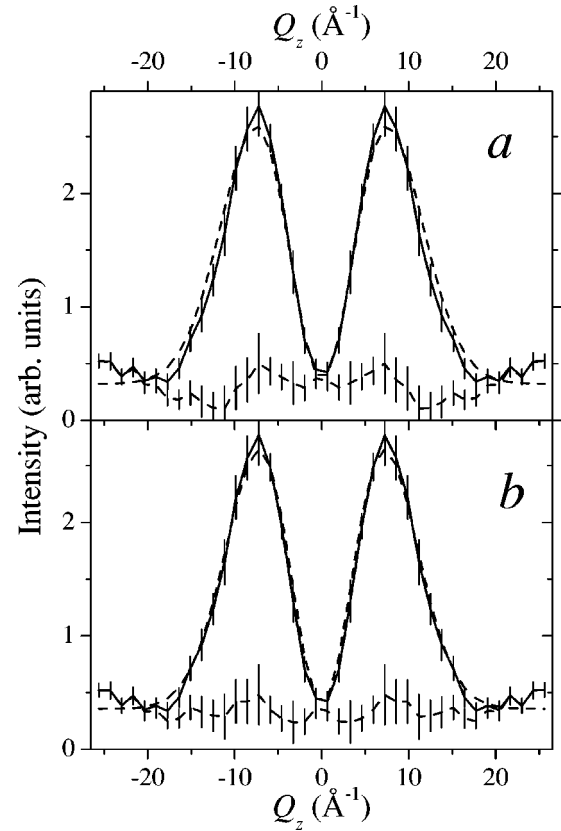


FIG. 10. Cut of $S(Q_x, Q_z, 960)$ at $Q_x=0$. Comparison of the measured profiles (solid lines with error bars) to harmonic profiles (dash line), calculated with Eq. (3). (a) $u_{0z}^2 = 1.75 \times 10^{-2} \text{ \AA}^2$ ($\hbar\omega = 960 \text{ cm}^{-1}$ for an isolated proton). (b) Best fit obtained with $u_{0z}^2 = 1.95 \times 10^{-2} \text{ \AA}^2$ ($\hbar\omega = 860 \text{ cm}^{-1}$ for an isolated proton). The dashed lines with error bars are differences between observed and calculated profiles.

modes, $\langle u_\alpha^2 \rangle_l$, was carried out with the scattering function including the lattice Debye-Waller factor explicitly,

$$S_{n_\alpha}(Q_\alpha, \omega) = \frac{(Q_\alpha^2 u_{0\alpha}^2)^{n_\alpha}}{n_\alpha!} \exp[-Q_\alpha^2 (u_{0\alpha}^2 + \langle u_\alpha^2 \rangle_l)] \times \delta(\omega - n_\alpha \omega_{0\alpha}). \quad (8)$$

TABLE I. Estimated mean-square amplitudes in planes (Q_i, Q_j) at energy transfer E from the best fits to the observed profiles of intensity. The harmonic frequencies were estimated for isolated proton oscillators. Δ_i is the difference between the mean square amplitude derived from the best fit and that for an isolated harmonic oscillator at the same frequency with an effective mass of 1 amu.

(Q_i, Q_j)	$E \text{ (cm}^{-1}\text{)}$	Transition	$u_x^2 (10^{-2} \text{ \AA}^2)$	$\hbar\omega_x \text{ (cm}^{-1}\text{)}$	Δ_x	$u_y^2 (10^{-2} \text{ \AA}^2)$	$\hbar\omega_y \text{ (cm}^{-1}\text{)}$	Δ_y	$u_z^2 (10^{-2} \text{ \AA}^2)$	$\hbar\omega_z \text{ (cm}^{-1}\text{)}$	Δ_z
$\gamma \text{ OH } (Q_x, Q_z)$	960 ± 40	$ 000\rangle \rightarrow 001\rangle$	0.95 ± 0.10	1760 ± 200	0.30 ± 0.10	1.95 ± 0.10	860 ± 50	0.20 ± 0.10
$\gamma \text{ OH } (Q_y, Q_z)$	960 ± 40	$ 000\rangle \rightarrow 001\rangle$	1.40 ± 0.10	1200 ± 70	0.17 ± 0.10	2.07 ± 0.10	810 ± 50	0.32 ± 0.10
$2 \times \gamma \text{ OH } (Q_x, Q_z)$	1840 ± 40	$ 000\rangle \rightarrow 002\rangle$	1.05 ± 0.10	1600 ± 150	0.40 ± 0.10	2.00 ± 0.10	840 ± 50	0.25 ± 0.10
$\delta \text{ OH } (Q_x, Q_y)$	1360 ± 40	$ 000\rangle \rightarrow 010\rangle$	1.05 ± 0.10	1600 ± 150	0.40 ± 0.10	1.48 ± 0.10	1130 ± 80	0.25 ± 0.10
$\delta \text{ OH } (Q_x, Q_z)$	1360 ± 40	$ 000\rangle \rightarrow 010\rangle$	1.49 ± 0.10	1125 ± 80	0.26 ± 0.10	1.85 ± 0.10	905 ± 50	0.10 ± 0.10
$\delta \text{ OH } (Q_x, Q_y)$	1600 ± 40	$ 000\rangle \rightarrow 010\rangle$	1.20 ± 0.20	1400 ± 200	0.20 ± 0.20
$\nu \text{ OH } (Q_x, Q_y)$	2560 ± 40	$ 000\rangle \rightarrow 100\rangle$ $ 000\rangle \rightarrow 020\rangle$	0.97 ± 0.10	1730 ± 200	0.32 ± 0.10	1.59 ± 0.10	1050 ± 100	0.36 ± 0.10

The best fits to the data gave $\langle u_\alpha^2 \rangle_l$ values very similar to the Δ_α 's given in Table I.

For a crystal free of static disorder like KHCO_3 at low temperature, the thermal factors derived from diffraction techniques are representative of the lattice dynamics. The thermal factors for the H atoms determined from neutron diffraction data at 14 K (Ref. 17) are: $\langle u_x^2 \rangle_{\text{diff}} = 1.34 \times 10^{-2} \text{ \AA}^2$, $\langle u_y^2 \rangle_{\text{diff}} = 1.54 \times 10^{-2} \text{ \AA}^2$, and $\langle u_z^2 \rangle_{\text{diff}} = 1.72 \times 10^{-2} \text{ \AA}^2$, with mean-square deviations of $\approx 2 \times 10^{-4} \text{ \AA}^2$. For the bending modes these values are virtually equal to those anticipated for harmonic proton oscillators. They are very similar to those estimated from incoherent elastic scattering given in Table I. For the stretching mode the discrepancy is greater but the INS data may be not sufficiently accurate to be conclusive.

B. Anharmonic coupling

For hydrogen bonds anharmonic coupling may contribute to complex band shaping mechanisms, like Fermi resonance.^{18–20,28,29} As long as interdimer coupling terms are ignored, the local potential for a dimer entity can be expanded as

$$V(x, y, z, \dots) = V_0(x, y, z, \dots) + W_{11}(x, y, z, \dots) \\ + W_{12}(x, y, z, \dots) + \dots$$

V_0 is the harmonic part of the potential expressed with normal coordinates x, y, z, \dots , and W_{11}, W_{12}, \dots are anharmonic perturbation terms of different orders.

In the ground state, the zero-order wave function can be factorized as ${}^0\Psi_0(x){}^0\Psi_0(y){}^0\Psi_0(z)\dots$. Within perturbation theory, the zero-order harmonic wave functions in the first excited states of x , ${}^0\Psi_1(x)$, and y , ${}^0\Psi_1(y)$, are mixed by antisymmetric anharmonic coupling terms in W_{11} as

$${}^1\Psi_1(x, y) = p_{11}{}^0\Psi_1(x) + q_{11}{}^0\Psi_1(y), \\ {}^2\Psi_1(x, y) = -q_{11}{}^0\Psi_1(x) + p_{11}{}^0\Psi_1(y), \quad (9)$$

with $p_{11}^2 + q_{11}^2 = 1$. The zero-order energy levels E_{x1}^0 and E_{y1}^0 are shifted apart to E_{11}^+ and E_{11}^- ,³⁰

$$E_{11}^\pm = \frac{1}{2}(E_{x1}^0 + E_{y1}^0) \pm \sqrt{\frac{1}{4}(E_{x1}^0 - E_{y1}^0)^2 + |W_{11}^{xy}|^2}, \quad (10)$$

with $W_{11}^{xy} = \langle {}^0\Psi_1(x) | W_{11}(x, y) | {}^0\Psi_1(y) \rangle$. If both x and y are proton coordinates, then

$$S(Q_x, Q_y, \omega) = |p_{11} \langle {}^0\Psi_0(x) | \exp(iQ_x x) | {}^0\Psi_1(x) \rangle \\ + q_{11} \langle {}^0\Psi_0(y) | \exp(iQ_y y) | {}^0\Psi_1(y) \rangle|^2 \\ \times \delta(\hbar\omega - E_{11}^+) \\ + | -q_{11} \langle {}^0\Psi_0(x) | \exp(iQ_x x) | {}^0\Psi_1(x) \rangle \\ + p_{11} \langle {}^0\Psi_0(y) | \exp(iQ_y y) | {}^0\Psi_1(y) \rangle|^2 \\ \times \delta(\hbar\omega - E_{11}^-). \quad (11)$$

Since all matrix elements are imaginary we obtain

$$S(Q_x, Q_y, \omega) = \{ p_{11}^2 \bar{S}_{1_x}(Q_x) + q_{11}^2 \bar{S}_{1_y}(Q_y) \\ + 2p_{11}q_{11} \sqrt{\bar{S}_{1_x}(Q_x) \bar{S}_{1_y}(Q_y)} \} \delta(\hbar\omega - E_{11}^+) \\ + \{ q_{11}^2 \bar{S}_{1_x}(Q_x) + p_{11}^2 \bar{S}_{1_y}(Q_y) \\ - 2p_{11}q_{11} \sqrt{\bar{S}_{1_x}(Q_x) \bar{S}_{1_y}(Q_y)} \} \\ \times \delta(\hbar\omega - E_{11}^-). \quad (12)$$

The terms proportional to $p_{11}q_{11}$ account for interference effects between the coupled wave functions. The scattering function is no longer symmetrical with respect to Q_x and Q_y . On the basis of numerical simulations, we conclude that there is no evidence of such effects in the maps of intensity.

If one of the coordinates, say x , corresponds to proton displacements, say δOH , and the other coordinate corresponds to a CO_3 vibration with negligible contribution to the total intensity, Eq. (12) gives

$$S(Q_x, \omega) = p_{11}^2 \bar{S}_{1_x}(Q_x) \delta(\hbar\omega - E_{11}^+) \\ + q_{11}^2 \bar{S}_{1_x}(Q_x) \delta(\hbar\omega - E_{11}^-). \quad (13)$$

The anharmonic coupling gives simple redistribution of the proton intensity among the perturbed levels. This equation has some similarity with Eq. (7) but the complex mixing of the δOH with two (ν_a and ν'_a) CO_3 coordinates is beyond the two-state approximation used in this section.

C. Fermi resonance

Fermi resonance between the OH stretching mode and the δOH overtone occurs when the zero-order wave functions ${}^0\Psi_1(x)$ and ${}^0\Psi_2(y)$ are mixed by anharmonic terms in W_{12} , in the same way as in Eq. (9)

$${}^1\Psi_{12}(x, y) = p_{12}{}^0\Psi_1(x) + q_{12}{}^0\Psi_2(y), \\ {}^2\Psi_{12}(x, y) = -q_{12}{}^0\Psi_1(x) + p_{12}{}^0\Psi_2(y), \quad (14)$$

with $p_{12}^2 + q_{12}^2 = 1$. The zero-order energy levels E_{x1}^0 and E_{y2}^0 are shifted to E_{12}^+ and E_{12}^- .³¹ The scattering function is analogous to Eq. (11), but the matrix elements are now either real or imaginary and terms proportional to $p_{12}q_{12}$ vanish,

$$S(Q_x, Q_y, \omega) = [p_{12}^2 \bar{S}_{1_x}(Q_x) + q_{12}^2 \bar{S}_{2_y}(Q_y)] \delta(\hbar\omega - E_{12}^+) \\ + [q_{12}^2 \bar{S}_{1_x}(Q_x) + p_{12}^2 \bar{S}_{2_y}(Q_y)] \delta(\hbar\omega - E_{12}^-). \quad (15)$$

Fermi resonance is a simple redistribution of the total intensity among the two levels. If the two states are not resolved the map of intensity is a superposition of the scattering functions for each transition. This is exactly what is observed in Fig. 9 and it is not possible to conclude whether Fermi resonance takes place or not. If it does occur, the splitting is certainly smaller than the actual resolution of $\pm 40 \text{ cm}^{-1}$.

VI. CONCLUSION

The observed maps of intensity are very similar to those anticipated for harmonic proton oscillators parallel to the main axes of the dimer entities. There is no visible mixing of the proton coordinates with internal coordinates for heavy atoms and the proton bending modes are largely decoupled from the lattice dynamics. The bands at 1360 and 1600 cm^{-1} appear as pure δ OH modes with effective masses of 1 amu. The INS scattering function of KHCO_3 is very close to that of a crystal of protons in a virtually rigid and transparent matrix. These dynamics are quite in accordance with previous normal mode analysis of the INS spectrum.²¹ Furthermore, the new assignment scheme for the INS band at 1600 cm^{-1} emphasizes the decoupling of the δ OH vibration. The physical origin of the decoupling of the proton dynamics is still largely opened to discussion³² and deserves further investigations.

In contrast to the normal mode analysis for dimensionless particles within the framework of classical mechanics, the

maps of intensity emphasize the quantal character of the proton dynamics. The vibrational ground state can be represented with three isolated harmonic oscillators along the coordinates imposed by the local symmetry of the hydrogen bonds. In excited vibrational states, combinations of the wave functions due to anharmonic coupling terms may arise. Such anharmonic mixing of the wave functions is actually observed for the δ OH and ν CO₃ coordinates. As the INS technique probes specifically the part of the wave function along the δ OH coordinate, the intensity arising from δ OH displacements is distributed among the states and the effective oscillator mass is always very close to 1 amu for each transition. On the other hand, optical techniques (infrared and Raman) probe primarily the part of the wave function along the CO₃ coordinates, but they do not probe the effective oscillator mass. This emphasizes the complementarity of the techniques: bands observed at the same frequency with INS and optical techniques may correspond to different parts of the wave function and must be compared with caution.

*Author to whom correspondence should be addressed. Electronic address: fillaux@glvt-cnrs.fr

¹E. B. Wilson, J. C. Decius, and P. C. Cross, *Molecular Vibrations* (McGraw-Hill, New York, 1964).

²P. Barchewitz, *Spectroscopie Infrarouge* (Gautier-Villars, Paris, 1967).

³S. J. Cyvin, *Molecular Vibrations and Mean-Square Amplitudes* (Elsevier, Amsterdam, 1968).

⁴A. I. Kitaigorodsky, *Molecular Crystals and Molecules* (Academic, New York, 1973).

⁵S. Califano, V. Schettino, and N. Neto, *Lattice Dynamics of Molecular Crystals* (Springer Verlag, Berlin, 1981).

⁶A. J. Pertsin and A. I. Kitaigorodsky, *The Atom-Atom Potential Method*, Springer Series in Chemical Physics (Springer Verlag, Berlin, 1987).

⁷A. C. Zemach and R. J. Glauber, *Phys. Rev.* **101**, 118 (1956).

⁸H. Jobic, J. Tomkinson, and A. Renouprez, *Mol. Phys.* **39**, 989 (1980).

⁹H. Jobic, R. E. Ghosh, and A. Renouprez, *J. Chem. Phys.* **75**, 4025 (1981).

¹⁰A. Griffin and H. Jobic, *J. Chem. Phys.* **75**, 5940 (1981).

¹¹H. Jobic and H. Lauter, *J. Chem. Phys.* **88**, 5450 (1988).

¹²G. J. Kearley, *J. Chem. Soc., Faraday Trans. 2* **82**, 41 (1986).

¹³S. W. Lovesey, *Nuclear Scattering, Theory of Neutron Scattered from Condensed Matter* (Clarendon, Oxford, 1984).

¹⁴M. Warner, S. W. Lovesey, and J. Smith, *Z. Phys. B: Condens. Matter* **51**, 109 (1983).

¹⁵J. O. Thomas, R. Tellegren, and I. Olovsson, *Acta Crystallogr.*,

Sect. B: Struct. Crystallogr. Cryst. Chem. **30**, 1155 (1974).

¹⁶J. O. Thomas, R. Tellegren, and I. Olovsson, *Acta Crystallogr.*, Sect. B: Struct. Crystallogr. Cryst. Chem. **30**, 2540 (1974).

¹⁷A. Cousson and W. Paulus (unpublished).

¹⁸A. Novak, P. Saumagne, and L. D. C. Bock, *J. Chim. Phys. Phys.-Chim. Biol.* **60**, 1385 (1963).

¹⁹K. Nakamoto, Y. A. Sarma, and K. Ogoshi, *J. Chem. Phys.* **43**, 1177 (1965).

²⁰G. Lucazeau and A. Novak, *J. Raman Spectrosc.* **1**, 573 (1973).

²¹F. Fillaux, J. Tomkinson, and J. Penfold, *Chem. Phys.* **124**, 425 (1988).

²²S. Kahsida, S. Ikeda, and Y. Nakai, *J. Phys. Soc. Jpn.* **63**, 4643 (1994).

²³S. Ikeda and F. Fillaux, *Phys. Rev. B* **59**, 4134 (1999).

²⁴<http://www.isis.rl.ac.uk/molecularspectroscopy/tosca/>.

²⁵S. Ikeda, M. Furusaka, T. Fukunaga, and A. D. Taylor, *J. Phys.: Condens. Matter* **2**, 4675 (1990).

²⁶<http://www.isis.rl.ac.uk/excitations/mari/>.

²⁷S. M. Bennington and R. S. Eccleston, Technical Report, ISIS Facility (1994).

²⁸F. Fillaux, *Chem. Phys.* **74**, 405 (1983).

²⁹A. Novak, *Struct. Bonding (Berlin)* **18**, 177 (1974).

³⁰C. Cohen-Tannoudji, B. Diu, and F. Laloë, *Mécanique Quantique* (Hermann, Paris, France, 1977).

³¹G. Herzberg, *Molecular Spectra and Molecular Structure* (Van Nostrand, New York, 1964), Vol. 2.

³²F. Fillaux, *Physica D* **113**, 172 (1998).